Journal of The Electrochemical Society

The Electrochemical Society
Advancing solid state & electrochemical science & technology

OPEN ACCESS

Mitigating Chemo-Mechanical Failure in Li-S Solid State Batteries with Compliant Cathodes

To cite this article: Yuxun Ren *et al* 2022 *J. Electrochem. Soc.* **169** 060503

Journal of The Electrochemical Society, 2022 **169** 060503

Mitigating Chemo-Mechanical Failure in Li-S Solid State Batteries with Compliant Cathodes

Yuxun Ren,[1] Nicholas Hortance,[1] and Kelsey B. Hatzell[1,2,3,z]

[1]*Department of Mechanical Engineering, Vanderbilt University, Nashville, Tennessee, 37240, United States of America*
[2]*Department of Mechanical and Aerospace Engineering, Princeton University, Princeton, New Jersey, 08540, United States of America*
[3]*Andlinger Center for Energy and Environment, Princeton University, Princeton, New Jersey, 08540, United States of America*

Solid-state sulfur cathodes based on inorganic sulfide solid electrolytes can enable energy-dense lithium batteries. However, volume changes and chemical decomposition can drive delamination and degradation during cycling. To overcome these challenges, this paper reports an in situ approach to encapsulate the solid-state sulfur cathode with a gel polymer electrolyte (GPE). The GPE is covalently bonded with the sulfide solid electrolyte and acts as a barrier that suppresses chemical decomposition between the sulfide solid electrolyte and cathode active material. The elastic GPE maintains interfacial contact within the sulfur cathode allowing for greater sulfur utilization. The solid-state sulfur cathode with GPE demonstrates capacities nearing 700 mAh g^{-1} and capacity retention over 100 cycles.

 [DOI: 10.1149/1945-7111/ac64cb]

Manuscript submitted January 23, 2022; revised manuscript received April 4, 2022. Published June 2, 2022. *This paper is part of the JES Focus Issue on Women in Electrochemistry.*

Supplementary material for this article is available online

There is increasing interest in safe, energy-dense, low-cost energy storage systems for electric vehicle and long duration energy storage.[1–4] Lithium-sulfur (Li-S) batteries have a theoretical capacity 6×(2600 W h kg^{-1}) greater than conventional lithium-ion batteries.[1,5] However, sulfur cathodes suffer from low ionic and electronic conductivity[6] and poor coulombic efficiency. Lithium polysulfides form as intermediate products during discharge and can react with lithium metal and dissolve in the liquid electrolyte.[2,7–9] The use of a liquid electrolyte leads to greater flammability and dilutes the active material content or loading.[10] Hybrid inorganic-organic solid-state sulfur cathodes may enable microstructure control, high active material loading, and decrease cell flammability. Exquisite control over cathodes microstructure is paramount for achieving good solid-phase ionic conductivity, mitigating lithium polysulfide dissolution, and resolving safety issues.[11–14]

A solid-state sulfur cathode combines elemental sulfur, a solid electrolyte, a conductive additive, and a binder. Inorganic sulfide solid electrolytes including lithium thiophosphate Li_2S-P_2S_5 (LPS),[3,15] argyrodite Li_6PS_5Cl,[16,17] and thio-LISICON-type $Li_{10}GeP_2S_{12}$,[18] can potentially meet the requirements for sulfur cathodes due to their transport ($\sigma_i = 10^{-2} \sim 10^{-4}$ S cm^{-1})[19] and mechanical properties (10 ∼ 30 GPa Young's modulus, 130 MPa yield strength).[20–23] In addition, sulfide-based solid electrolytes can be processed using scalable liquid-phase approaches[13,24–26] and easily infiltrated into porous carbon scaffolds with elemental sulfur.[6,24,27] While there is great interest in solid-state cathodes, long-term cycling has had limited success due to a range of chemo-mechanical degradation processes[1,28] that drive delamination, fracture, and chemical decomposition.[3,29,30] Sulfur undergoes a significant volume expansion (80%) during lithiation, which results in large strains in the cathode.[14,31–34] Thus, compliant interfaces between individual components in a composite cathode is critical to avoid chemo-mechanical degradation over cycle lifetime.[35,36] In addition to chemo-mechanical degradation, chemical decomposition is also a significant challenge to overcome because sulfide solid electrolytes are thermodynamically unstable and prone to decompose when in contact with the conductive additive.[37,38]

Herein, we propose a composite sulfur cathode architecture which combines two ion-conducting phases. The gel polymer electrolyte (GPE) is effectively crosslinked with a sulfide solid electrolyte (lithium thiophosphate, LPS).[32] Experimental results reveal that the bonding between GPE and LPS suppresses LPS dissolution and decomposition. Modeling demonstrates the importance of the elastic gel polymer electrolyte on maintaining interfacial contact within the solid-state sulfur cathode. Overall, the gel polymer electrolyte serves two important functions: (1) suppresses chemical decomposition of the solid electrolyte, and (2) enables for electrode compliance over cycling. Solid-state sulfur cathodes with gel polymer electrolytes can achieve improved cycling with a practical sulfur loading (2.5 mg cm^{-2}) and electrolyte/sulfur mass ratio (3).

Experimental Section

Materials Synthesis.—Li_2S(99%), P_2S_5 (99%), sulfur (99%), anhydrous tetrahydrofuran (THF, 99.9%), tetraglyme (G4) were obtained from Fisher Scientific and used as received. Lithium metal (99.9%), pentaerythritol tetraacrylate (PETEA), carbon nanofiber (CNF, diameter 100 nm, length 20–200 μm), polytetrafluoroethylene (PTFE), and azobisisobutyronitrile (AIBN) were obtained from Sigma-Aldrich. Li_2S and P_2S_5 were mixed with a molar ratio of 3:1 in THF (360 mg solid in 1.0 ml solvent) at room temperature for 12 h. The precipitate was collected by centrifugation and washed with THF three times. The collected powder was dried in argon atmosphere for 12 h at room temperature and further dried for 1 h at 50 °C. After drying, Li_3PS_4·3THF was obtained and thermally treated at 200 °C in argon for 2 h to obtain Li_2S-P_2S_5 (LPS) electrolyte.[15]

Composite cathodes (with varying LPS:S mass ratios) were processed by combining LPS, sulfur, carbon nanofiber, and PTFE with a mass ratio of 3:2:0.8:0.2 (LPS:S = 1.5) or 6:2:0.8:0.2 (LPS:S = 3) in THF (300 mg solid in 3.0 ml solvent). The slurry was stirred for 12 h and THF was evaporated at room temperature in an argon filled glove box. Once the solvent was evaporated, the composite was thermally treated at 50 °C for 1 h. Powders were subsequently pressed onto a 10 mm-diameter Al foil at a pressure of 160 MPa and heated at 80 °C for 2 h and 100 °C for 2 h to remove excess solvent and convert Li_3PS_{4+x} to separated LPS and sulfur.

[z]E-mail: kelsey.hatzell@princeton.edu

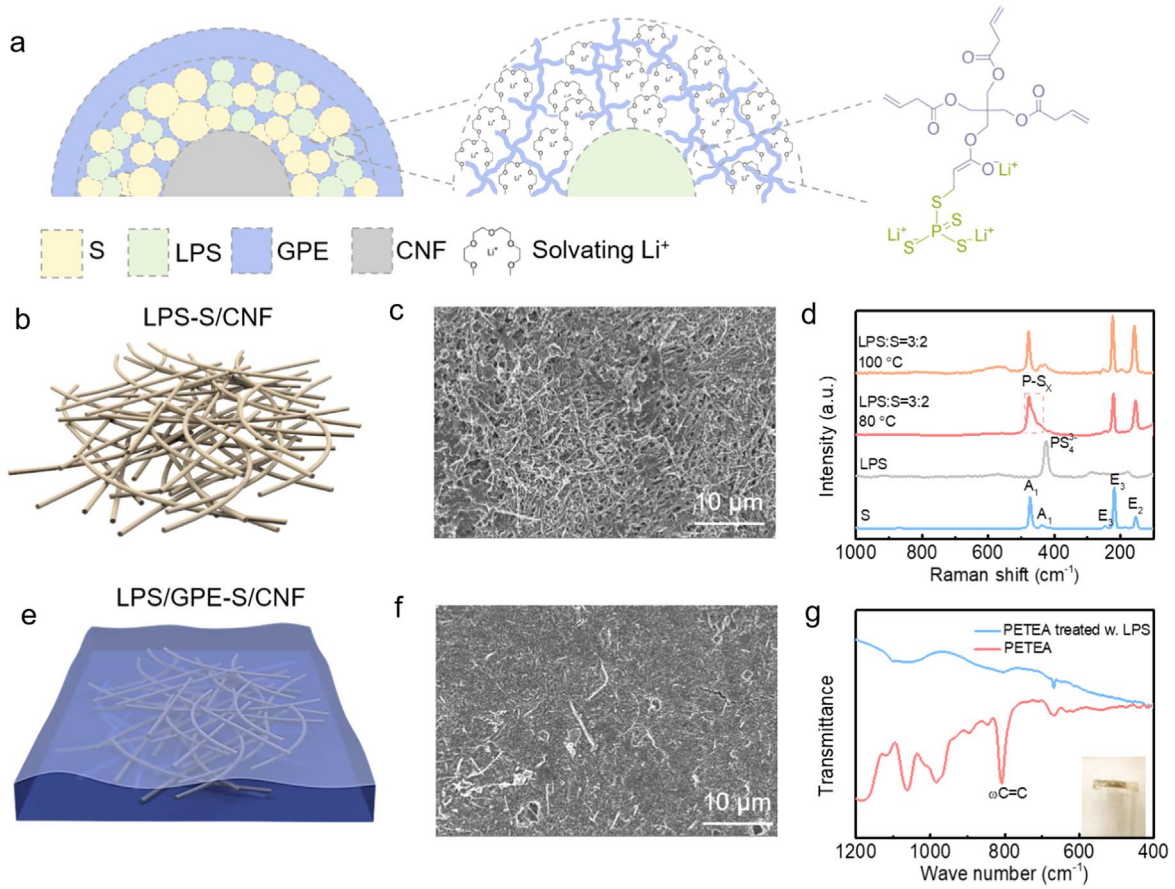

Figure 1. In situ gel polymer electrolyte encapsulation. (a) Schematic showing the electrode compositions (left to right: crosssection of a fiber in the electrode, LPS particle grafted with gel polymer electrolyte, the crosslinked LPS/PETEA). (b) Schematic of the LPS-S/CNF electrode. (c) SEM image of the LPS-S/CNF electrode. (d) Raman spectra of the electrode heat treated at different temperatures. (e) Schematic of the LPS/GPE-S/CNF electrode. (f) SEM image of the LPS/GPE-S/CNF electrode. (g) FTIR of the crosslinked and pristine PETEA, the inset photo shows the PETEA gel crosslinked by LPS.

When LPS:S = 1.5, the electrode thickness was around 66 μm, and the areal sulfur loading was 2.5 mg cm^{-2}, taking up 19% volume of the electrode.

Composite solid sulfur cathodes were constructed with and without the gel polymer electrolyte. A solution of LiTFSI and tetraglyme (G4) was formulated with a 1:1 molar ratio and is referred to as LiG4 in the text. The liquid precursor for gel polymer electrolyte is composed of a solution of LiG4 (94.0 $\sim$ 79.0 wt%), pentaerythritol tetraacrylate (PETEA) (5.0 $\sim$ 20.0 wt%), and azobisisobutyronitrile (AIBN) (1.0 wt%). The effect of crosslinking monomer (PETEA) concentration (5.0, 10.0 or 20.0 wt%) was studied to understand how the extent of crosslinking affected ionic conductivity and battery performance. 3.0 mg of liquid precursor was dropped onto the electrode (LPS-S/CNF). The electrode was held in vacuum for 1 h to enable the liquid infiltration in the electrode and then heat treated at 80 °C for 2 h to form the LPS/GPE-S/CNF. The PETEA will spontaneously react with LPS via thiol-ene reaction. The AIBN initator will further crosslink the residual PETEA in the liquid precursor at 80 °C.

To fabricate the electrode for stability evaluation, LPS, CNF and PTFE were hand grounded with a mass ratio of 3:1.6:0.4, and the powder (10.0 mg) was pressurized at 160 MPa to form an electrode (10 mm in diameter). 6.0 mg pure LiG4 or LiG4 with additive (10.0 wt% PETEA 1.0 wt% AIBN) would be added respectively onto the electrode, followed by the same treatment for the sulfur cathode.

Battery assembly and test.—Li-S batteries were assembled with modified Li metal foil (0.5 mm Li in thickness), Celgard 2500 separator (18 mm in diameter), and the composite cathode. The Celgard separator was filled with the GPE prior to assembly to enable a good contact with the electrodes. The liquid-type precursor solution consisted of 94.0wt% LiG4, 5.0 wt% PETEA, and 1 wt% AIBN. The GPE loading on each separator was 3 μl cm^{-2}. All Li metal was treated prior to cell assembly. The Li foil was cleaned and punched into 12 mm in diameter disks and subsequently submersed into a 50 mM BiF_3-P_2S_5 in tetraglyme solution for 1 h. Next, the treated Li foil was dried at 120 °C for 1 h, and pressed at 10 MPa for 3 min.

Materials characterization.—The solid electrolyte was analyzed by powder X-ray diffraction (Rigaku Smartlab, Tokyo, Japan) with a step of 5° min^{-1}. The compositions of solid electrolytes and electrodes examined by Raman (Thermofisher) with a wavelength of 532 nm. The functional group of polymer was examined by Fourier transform infrared spectroscopy. Thermal stability of polymer was evaluated by thermogravimetric analyzer with a heating rate of 20 °C min^{-1}. The morphology and species distribution were examined by field emission scanning electron microscope (Zeiss Merlin, Oberhochem, Germany).

Results and Discussion

Hybrid inorganic-organic solid state cathode.—A composite solid-state sulfur cathode combines an inorganic solid electrolyte (Li_2S-P_2S_5 or LPS), a compliant gel polymer electrolyte (GPE), an electrically conducting carbon fiber matrix, and elemental sulfur (1675 mAh g^{-1}) (Figs. 1a, 1b and 1e). Polymers binders can dampen mechanical strain induced upon cycling and prevent electrode fracture. However, conventional polymer binders are ion-insulating and can delaminate from the active material.[39] An

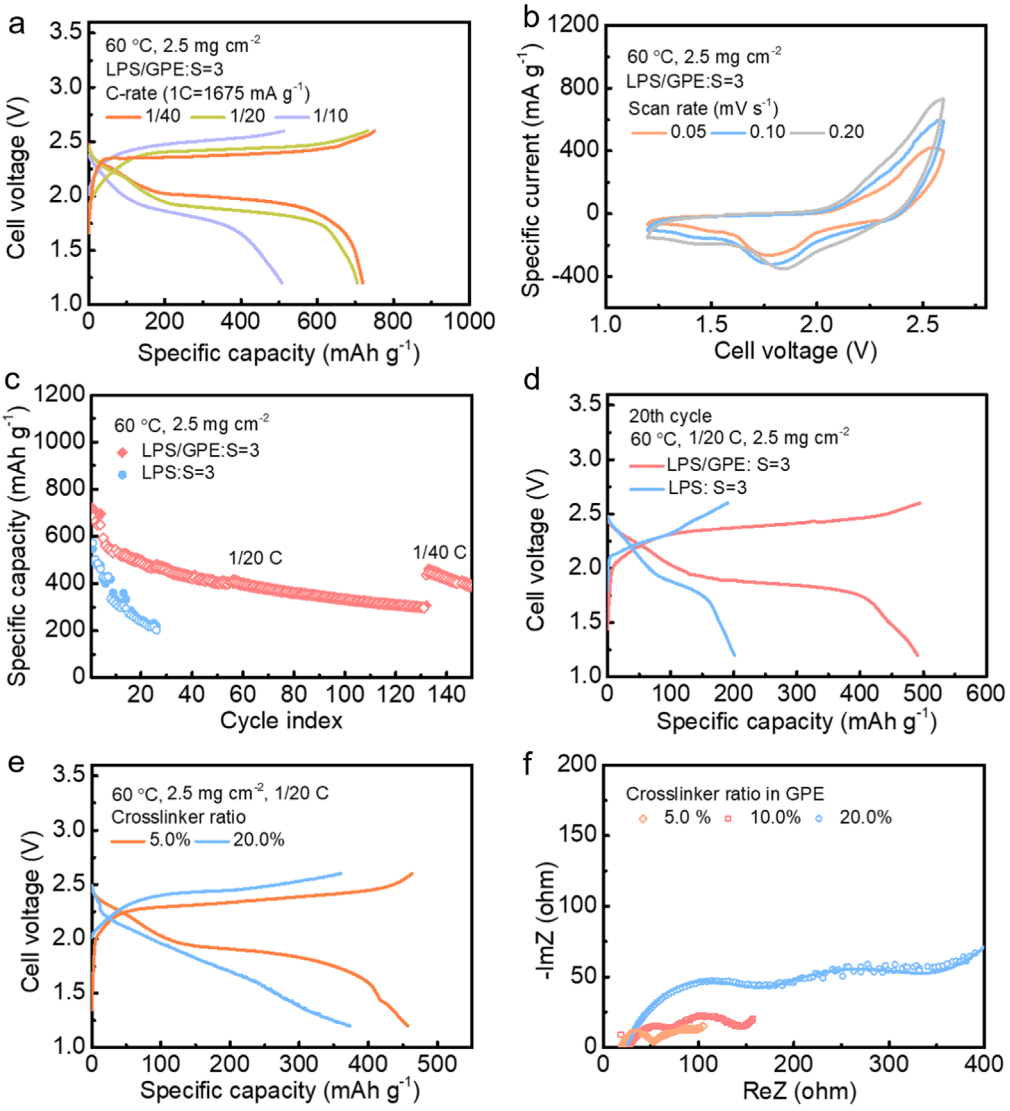

Figure 2. Performance of the composite sulfur cathode. (a) Voltage profiles of Li-S batteries using LPS/GPE electrolyte (LPS/GPE:S = 3 in wt) with a sulfur loading of 2.5 mg cm^2 at 60 °C. (b) CV profiles at different rates. (c) Cycling performance at 1/20 C for batteries using LPS (LPS:S = 3 wt) and LPS/GPE electrolyte. (d) Corresponding voltage profiles. (e) Voltage profiles achieved using different monomer ratios in the GPE of the hybrid electrolyte. (f) Corresponding EIS profiles measured after charging at the 5th cycle. The electrical circuit model of EIS and fitting details can be found in Fig. S12.

alternative strategy to traditional binders is the use of a gel polymer electrolyte which can improve the electrode elasticity, act as a barrier for chemical decomposition, and improve cell cycle life (Figs. 1a, 1b and 1e).

Sulfide-containing solid electrolyte (LPS, $\sigma_i = 0.59$ mS cm^{-1} at 60 °C, available at stacks.iop.org/JES/169/060503/mmedia Fig. S 1) and sulfur will spontaneously form soluble Li_3PS_{4+x} species (x = 3.74) when combined in tetrahydrofuran (THF).[24] This soluble product (Li_3PS_{4+x}) can be directly processed into a carbon matrix (carbon nanofiber) to create an all-inorganic solid state cathode (Figs. 1b, c, S2). Nano-sizing sulfur and LPS leads to good transport properties. Upon heating (100 °C) the solid state cathodes demonstrates distinct Raman peaks at the LPS (470 cm^{-1}) and sulfur (476 and 347 cm^{-1}) peak (Fig. 1d). Sulfur aggregation (crystallization) can occur at a higher temperature but was not observed in the X-ray diffraction pattern (Fig. S3). The gel polymer electrolyte was introduced in a secondary process (Figs. 1e–1f). LPS is intrinsically reactive and can trigger the crosslinking of the gel polymer electrolyte and formation of a conformal coating on the active material (LPS/S) (Fig. 1a). In this work pentaerythritol tetraacrylate (PETEA) was used as the crosslinking monomer, and can be initiated by either radical or Lewis base.[40–42] The Lewis-basic PS_4^{3-} site on the solid electrolyte (LPS) can initiate the nucleophilic attack toward the C = C bond in PETEA (Fig. 1g) and link LPS with PETEA and convert the oxygen double bond into a Lewis basic oxonium ions. The oxonium ions will subsequently initiate the cross-linking between excess PETEA molecules (Fig. 1a). A decrease in the wagging (out of plane bending) peak for C = C bond is observed in the FTIR and confirms that the C = C bond (PETEA) reacts with LPS[40] (inset in Fig. 1g).

The GPE (10.0 wt% PETEA, 1.0 wt% azobisobutyronitrile, and 89.0 wt % solvate ionic liquid LiG4) was added directly to the solid state cathode and reacts with LPS. Subsequently, the electrode was heated to 80 °C to initiate radical-initiated polymerization[40] (Fig. 1a). The polymer matrix containing LiG4 liquid electrolyte is referred to as the gel polymer electrolyte (GPE), and the composite sulfur cathode using both LPS and GPE is designated by LPS/GPE-S/CNF. SEM images of the electrode surface and cross-section demonstrates uniform encapsulation of the fibrous electrodes by the GPE (Fig. 1f and Fig. S2). LiG4 was selected as the electrolyte in the GPE, because LiG4 has a good ionic conductivity (3.6 mS cm^{-1} at 60 °C, Fig. S4) and viscosity (81 mPa···).[43] In addition, LiG4

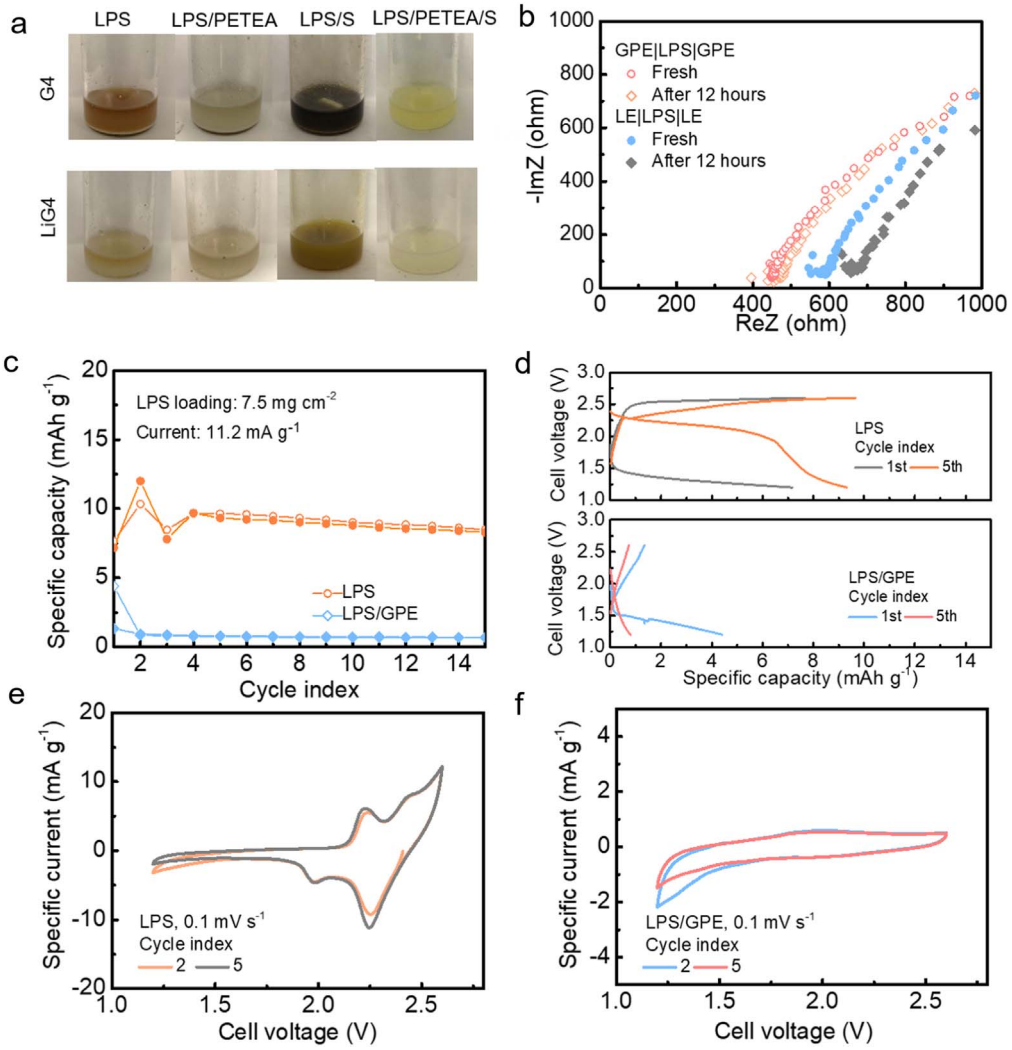

Figure 3. Suppressed dissolution and redox reaction of LPS. (a) Photos showing soaking of LPS (15 mg) in the solvents (G4 and LiG4, 1 ml), under condition with/without sulfur (10 mg), with/without PETEA (1.5 mg). (b) Nyquist plots of the LPS pellet and trilayer cell. (c) Cyclability of the half cells using Li_3PS_4 as the active material, with and without the treatment of PETEA. (d) Corresponding voltage profiles. (e, f) Cyclic voltammetry profiles (after galvanostatic cycling).

exhibits low solubility to lithium polysulfides (LiPS) and the solid electrolyte LPS.[44] Finally, the GPE demonstrates good thermal stability up to 200 °C (Fig. S5).

Full-cell performance.—Full cells were constructed to evaluate the electrochemical performance of the inorganic-organic solid state cathodes. The lithium metal anode was protected with a coating comprised of Li_3Bi and LiF in order to suppress anode reactions.[45] The GPE infiltrated into a Celgard membrane to form a quasi-solid-state separator. Symmetric cell (Li|GPE|Li) experiments demonstrated good stability at 0.8 mA cm^{-2} (0.8 mAh cm^{-2}) (Fig. S6). In full cell experiments, the battery demonstrated a specific capacity of 720, 700 and 510 mAh g^{-1} (Fig. 2a) at C/40, C/20 and C/10 (1 C = 1675 mA g^{-1}, based on sulfur). A single, flat plateau at 2.1 V was observed at all rates. This was also observed in the cyclic voltammetry (CV) profiles, where there was only one cathodic peak centered at 1.75 V (Fig. 2b). Ex situ Raman microscopy observed the formation of Li_2S at the early stage of discharge (100 mAh g^{-1}, C/10, 20 % depth of discharge), but there was no signal of lithium polysulfide intermediates (Fig. S7). This implies that sulfur redox reaction follows a solid-solid phase transformation process, rather than the conventional solid-liquid-solid process observed in Li-S batteries using liquid electrolytes (Fig. S8).[10]

Different electrolytes (LPS, GPE and LPS/GPE) were integrated into solid state cathodes and characterized electrochemically (Fig. 2c, d and Fig. S9). The composite sulfur cathode using LPS electrolyte (LPS:S = 3 wt) experienced a large polarization (830 mV at C/20), a discharge voltage profile with a large slope (Fig. S9), and a significant capacity decay (34% capacity retention in 25 cycles). Rapid capacity decay is widely reported for the solid-state Li-S battery and ascribed to chemo-mechanical failure.[46] For the composite sulfur cathode using GPE electrolyte (GPE:S = 3 wt), the battery exhibited a low sulfur utilization (350 mAh g^{-1} at C/20). Although, the GPE provides a higher ion conductivity than LPS, it is difficult for the ion to transport within the bulk phase of sulfur (Fig. S10). In addition, rapid capacity decay was observed after 25 cycles, most likely due to LiPS dissolution in GPE, and corrosion of Li anode.[46] The LPS/GPE-S/CNF cathode demonstrated 75% capacity retention over 25 cycles, and 50% capacity retention over 130 cycles (Fig. 2c, 2d). Subsequently, the specific capacity returned to around 500 mAh g^{-1} (71% of the initial capacity) when the charge rate was decreased to C/40.

To systematically probe the role of mechanics on electrochemical properties, we modified the PETEA monomer ratio (Figs. 2e, 2f). The control eperiment with a pure LiG4 liquid electrolyte (LPS-S/CNF electrode) demonstrated an initial capacity near 800 mAh g^{-1} which decreased by 50% after 25 cycles (Fig. S11). As the monomer ratio increased from 5.0 wt.% to 20.0 wt.%, a subsequent increase in the overpotential, bulk resistance, and charge-transfer resistance was observed (Fig. 2e). The rise in the crosslinker fraction in the liquid

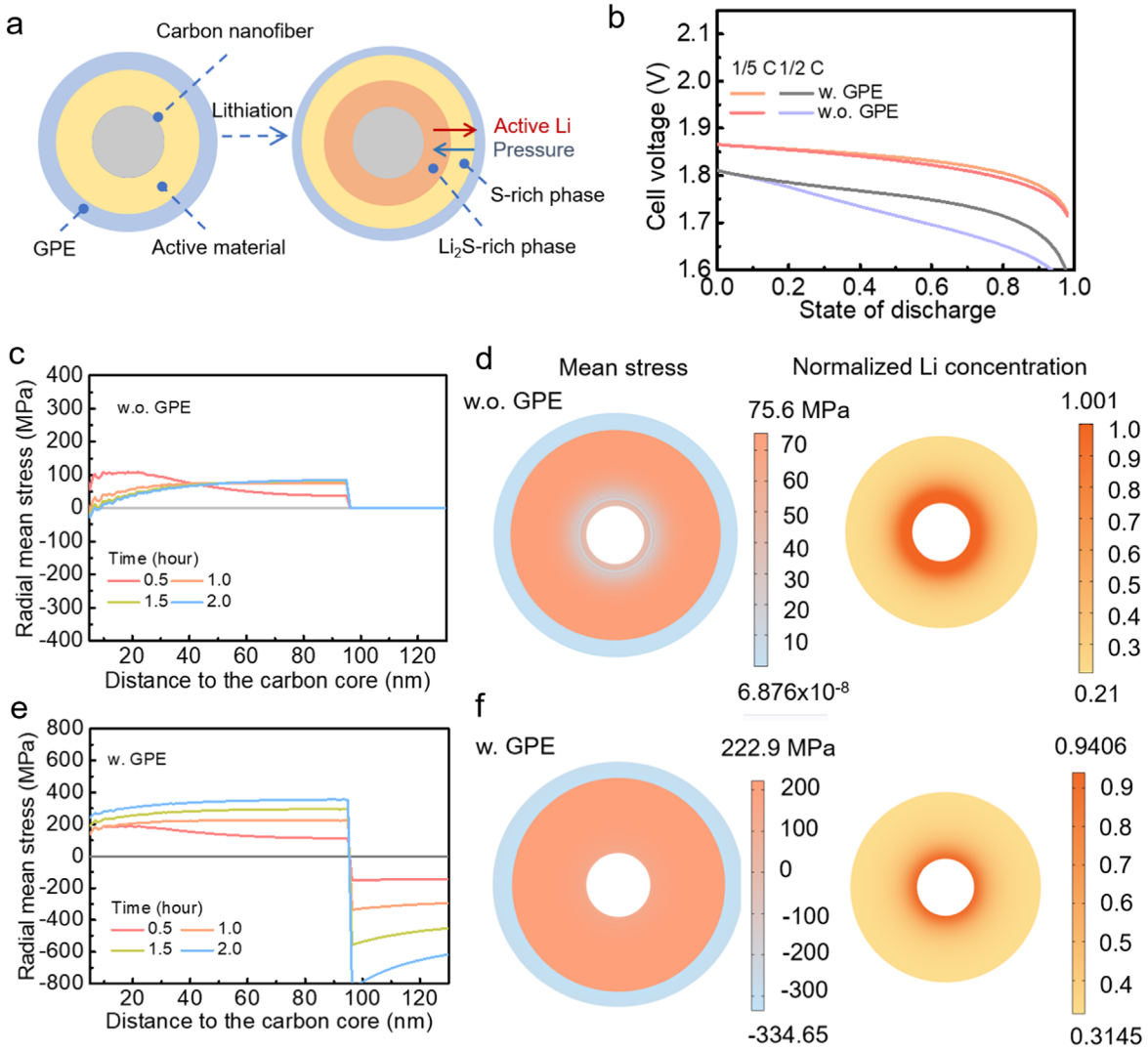

Figure 4. Chemomechanical simulation. (a) Schematic showing the effect of polymer coating on lithiation. (b) Discharge curves of the electrodes with and without polymer; (c, e) Radial mean stress distribution as a function of distance from the carbon core (displacement was not included).(d, f) Mean stress and active Li distributions (normalized) at a specific capacity of 837 mAh g^{-1}. The conditions without (c, d) and with (e, f) GPE are considered.

precursor results in a dense polymer skeleton after gelation and enhances Youngs modulus (stiffness) of the as-formed gel polymer electrolyte. The high-stiffness gel polymer electrolyte leads to a less intimate ionic contact and constrains the cathode volume expansion during lithiation (Fig. 2f, Fig. S12). A high monomer ratio can increase the Young's modulus (stiffness) of the composite cathode and constrain the cathode volume expansion during lithiation (Figs. 2f, and S12). Cycle lifetime demonstrates a non-linear relationship with monomer concentration with greatest performance observed for the electrode with 10.0 wt.% (Figs. 2c, S12). At low monomer concentrations (e.g. 5.0 wt.%), the LPS is not uniformly coated with the GPE and thus decomposition can drive capacity decay. At higher monomer concentrations (e.g. 20.0 wt.%), the composite cathode is too rigid and cannot accommodate large volume expansion. Thus, engineering the solid state cathodes for transport, chemistry, and mechanics is important for next generation solid state batteries.

Solid electrolyte decomposition and decreases in interfacial contact are the two predominant failure pathways for solid state batteries. To improve transport properties, hindered by delamination, many groups add a small amount of liquid electrolyte to the sulfur cathode. However, sulfide solid electrolytes have been known to dissolve or decompose in liquid electrolytes and thus is not a viable approach.[24,38] LPS reacts and decomposes readily in G4 which is visible by a solution color change (Fig. 3a). One strategy to reduce LPS dissolution is solvating more Li^+ in G4 to reduce Li^+ dissociation from LPS.[44] Another strategy is to create a protective barrier on the LPS so that it cannot get in contact with the liquid precursor. LPS covalantly bonded with PETEA avoidcvent (Fig. 3a). Trilayer (GPE|LPS|GPE or LE|LPS|LE cell) experiments were conducted to understand the role of chemical decomposition on the interfacial resistance (Fig. 3b, Fig. S13). The interfacial resistance between the liquid electrolyte (LiG4) and LPS is large and increases over time which is likely due to decomposition (Fig. 3b).[47] In contrast, the intefacial resistance between the GPE and LPS surface is stable with a small interfacial resistance (around 12 ohm cm^{-2} at 60 °C).

LPS exhibits a narrow stability window (1.71 ~ 2.31 V)[48] and can decompose into sulfur. Sulfur can further react with LPS to create soluble Li_3PS_{4+x}. Dissolution can be observed simply by blending LPS and sulfur in G4 and LiG4 by a brown color solution (Fig. 3a). After a protective barrier (polymer) is coated on LPS, the reaction between sulfur and LPS was greatly suppressed in G4. In LiG4 solution, there is almost no dissolution (Fig. 3a, Fig. S14). The covalent bonding between LPS and PETEA can increase the energy barrier for LPS reduction/oxidation. Stability tests on a trilayer (Li|LPS) half cell (LPS loading 7.5 mg cm^{-2}) demonstrated an

initial discharge capacity of 7.0 mAh g_{LPS}^{-1} (0.052 mAh cm^{-2} for the cell) and remained stable at 10 mAh g_{LPS}^{-1} during cycling (1.2–2.6 V). The initial discharge capacity for the trilayer with the GPE was significantly less suggesting greater stability (4.0 mAh g_{LPS}^{-1}, 0.03 mAh $cm^{-2}$for the cell) (Figs. 3c, 3d). In addition, the LPS electrode demonstrated redox peaks (at 2.2 V and 2.0 V) (Fig. 3e), whereas the LPS/GPE electrode had no visible redox peaks (Fig. 3f). According to the CV profile, it can be deduced that, without GPE, LPS is partially decomposed to sulfur and phosphorous sulfide species.[48] XRD and Raman characterizations revealed that the LPS/GPE electrode contained a small fraction of Li_2S (decomposition product) at the end of discharge that the LPS/Li trilayer (Fig. S15).

Chemo-mechanical implications on performance.—Maintaining the interfacial contact between sulfur and LPS is crucial for effective sulfur utilization. A finite element model coupling electrochemistry, transport, and mechanics was developed to study the impact of lithiation on chemo-mechanical properties of the sulfur cathode (model details presented in the supporting information). The cross Section of a single CNF fiber (radius $r = 50$ nm) coated with an annulus of active material (LPS/S, $r = 50 \sim 145$ nm) and an annulus of gel polymer electrolyte ($r = 145 \sim 180$ nm) was selected as the computational domain (Fig. S16, Fig. 4a). Low sulfur utilization is attributed to the low electronic conductivity of the active sulfur material ($\sigma_e = 10^{-10}$)[14,49,50] (Table S1). The lithiation reaction primarily occurs at the interface between the CNF (electron conductor) and LPS/S (active material) leaving sulfur located away from the core fiber unlithiated (Fig. 4a). The reaction front in the LPS/S cathode (no GPE) is observed to push the active material layer outward in order to release the lithiation-induced stress during discharge (Fig. 4c). The compressive stress at the interface between the carbon core and active material decreases to a negligible value after one h of discharge (C/2) (Fig. 4c). Thus, the active Li remains in the region close to the carbon core (Fig. 4d) which results in a larger overpotential (Fig. 4b).

The addition of an elastic GPE layer significantly changes the lithiation process in the cathode. First the cathode active material expands and results in the GPE stretching. This in turn imposes a compressive stress on the active material layer (Fig. S17) and pushes the active material inward (Fig. 4e). This compressive force results in better interfacial contact between S-rich shell and Li_2S-rich core and more homogeneous active Li distribution within the active material [51] (Fig. 4f). As a result, the stress-driven transport reduced the discharge overpotential and promoted the utilization ratioof sulfur (Fig. 4b).

Conclusions

Combining an inorganic sulfide solid electrolyte with a gel polymer electrolyte provides a pathway toward suppressing both chemical decomposition and chemo-mechanical failure in energy dense, conversion-type cathode materials. Herein, a gel polymer electrolyte was combined with an inorganic solid electrolyte and elemental sulfur to create a solid state cathode. The gel polymer electrolyte can act as a protective barrier for solid electrolyte chemical decomposition. The gel polymer also provides controlled mechanical propertiesl (elasticity) to accomodate large volume expansion processes reversible. The hybrid solid-state sulfur cathode achieved capacities around 800 mAh g^{-1} at C/20, 75% capacity retention over 25 cycles, and 50% capacity retention over 130 cycles. Chemical and electrochemical studies confirmed that the crosslinking approach effectively diminished chemical decomposition of the sulfide solid electrolyte. Chemo-mechanical simulation of the composite electrode emphasized the importance of maintaining intimate interfacial contact within solid-state sulfur cathode. The results demonstrate a general design strategy for solid-state sulfur cathodes, which simultaneously addresses chemical stability issues and chemo-mechanical challenges.

Acknowledgments

The authors were supported by the National Science Foundation under grant No. 1 847 029 and support from the Toyota Research Institute in North America. The authors acknowledge the Vanderbilt Institute of Nanoscience and Engineering (VINSE) for access to their shared characterization facilities.

ORCID

Kelsey B. Hatzell https://orcid.org/0000-0002-5222-7288

References

1. P. Bonnick, K. Niitani, M. Nose, K. Suto, T. S. Arthur, and J. Muldoon, "High performance all solid state lithium sulfur battery with lithium thiophosphate solid electrolyte." *Journal of Materials Chemistry A*, **7**, 24173 (2019).
2. K. B. Hatzell, X. C. Chen, C. Cobb, N. P. Dasgupta, M. B. Dixit, L. E. Marbella, M. T. McDowell, P. Mukherjee, A. Verma, and V. Viswanathan, "Challenges in lithium metal anodes for solid state batteries." *ACS Energy Lett.*, **5**, 922 (2020).
3. M. B. Dixit, N. Singh, J. P. Horwath, P. D. Shevchenko, M. Jones, E. A. Stach, T. S. Arthur, and K. B. Hatzell, "In Situ Investigation of Chemomechanical Effects in Thiophosphate Solid Electrolytes." *Matter*, **3**, 2138 (2020).
4. C. A. Fernandez, N. M. Hortance, Y.-H. Liu, J. Lim, K. B. Hatzell, and M. C. Hatzell, "Opportunities for intermediate temperature renewable ammonia electrosynthesis." *Journal of Materials Chemistry A*, **8**, 15591 (2020).
5. M. Li, J. E. Frerichs, M. Kolek, W. Sun, D. Zhou, C. J. Huang, B. J. Hwang, M. R. Hansen, M. Winter, and P. Bieker, "Solid-State LithiumSulfur Battery Enabled by Thio-LiSICON/Polymer Composite Electrolyte and Sulfurized Polyacrylonitrile Cathode." *Adv. Funct. Mater.*, **1910123**, 30 (2020).
6. F. Han, J. Yue, X. Fan, T. Gao, C. Luo, Z. Ma, L. Suo, and C. Wang, "High-performance all-solid-state lithiumsulfur battery enabled by a mixed-conductive Li2S nanocomposite." *Nano Lett.*, **16**, 4521 (2016).
7. P. G. Bruce, S. A. Freunberger, L. J. Hardwick, and J.-M. Tarascon, "LiO 2 and LiS batteries with high energy storage." *Nat. Mater.*, **11**, 19 (2012).
8. J. P. Mwizerwa, Q. Zhang, F. Han, H. Wan, L. Cai, C. Wang, and X. Yao, "Sulfur-Embedded FeS2 as a High-Performance Cathode for Room Temperature All-Solid-State LithiumSulfur Batteries." *ACS Applied Materials & Interfaces*, **12**, 18519 (2020).
9. M.-H. Ryou, Y. M. Lee, Y. Lee, M. Winter, and P. Bieker, "Mechanical surface modification of lithium metal: towards improved Li metal anode performance by directed Li plating." *Adv. Funct. Mater.*, **25**, 834 (2015).
10. Q. Pang, A. Shyamsunder, B. Narayanan, C. Y. Kwok, L. A. Curtiss, and L. F. Nazar, "Tuning the electrolyte network structure to invoke quasi-solid state sulfur conversion and suppress lithium dendrite formation in LiS batteries." *Nat. Energy*, **3**, 783 (2018).
11. A. Hayashi, T. Ohtomo, F. Mizuno, K. Tadanaga, and M. Tatsumisago, "All-solid-state Li/S batteries with highly conductive glassceramic electrolytes." *Electrochemistry communications*, **5**, 701 (2003).
12. Y. Liu, P. He, and H. Zhou, "Materials, Construction, and Challenges." *Adv. Energy Mater.*, **8**, 1701602 (2018).
13. M. B. Dixit, W. Zaman, Y. Bootwala, Y. Zheng, M. C. Hatzell, and K. B. Hatzell, "Scalable manufacturing of hybrid solid electrolytes with interface control." *ACS applied materials & interfaces*, **11**, 45087 (2019).
14. M. B. Dixit, M. Regala, F. Shen, X. Xiao, and K. B. Hatzell, "Tortuosity effects in garnettype Li7La3Zr2O12 solid electrolytes." *ACS applied materials & interfaces*, **11**, 2022 (2018).
15. Z. Liu, W. Fu, E. A. Payzant, X. Yu, Z. Wu, N. J. Dudney, J. Kiggans, K. Hong, A. J. Rondinone, and C. Liang, "Anomalous high ionic conductivity of nanoporous β- Li3PS4." *J. Am. Chem. Soc.*, **135**, 975 (2013).
16. C. Yu, L. van Eijck, S. Ganapathy, and M. Wagemaker, "Synthesis, structure and electrochemical performance of the argyrodite Li6PS5Cl solid electrolyte for Li-ion solid state batt." *Electrochimica Acta*, **215**, 93 (2016).
17. S. Yubuchi, S. Teragawa, K. Aso, K. Tadanaga, A. Hayashi, and M. Tatsumisago, "Preparation of high lithium-ion conducting Li6PS5Cl solid electrolyte from ethanol solution for all-solid-state lithium batteries." *Journal of Power Sources*, **293**, 941 (2015).
18. K. Yang, J. Dong, L. Zhang, Y. Li, and L. Wang, "An Effective Method to Enhance the Electrochemical Properties of Li10GeP2S12-Based Solid Electrolytes." *J. Am. Ceram. Soc.*, **98**, 3831 (2015).
19. Q. Zhang, D. Cao, Y. Ma, A. Natan, P. Aurora, and H. Zhu, "Sulfide-Based Solid-State Electrolytes: Synthesis, Stability, and Potential for All-Solid-State Batteries." *Adv. Mater.*, **31**, 1901131 (2019).
20. F. P. McGrogan, T. Swamy, S. R. Bishop, E. Eggleton, L. Porz, X. Chen, Y.-M. Chiang, and K. J. Van Vliet, "Compliant Yet Brittle Mechanical Behavior of Li2S P2S5 Lithium-Ion-Conducting Solid Electrolyte." *Adv. Energy Mater.*, **7**, 1602011 (2017).
21. Y. Yang, Q. Wu, Y. Cui, Y. Chen, S. Shi, R.-Z. Wang, and H. Yan, "Elastic properties, defect thermodynamics, electrochemical window, phase stability, and Li + mobility of Li3PS4: Insights from first-principles calculations." *ACS applied materials & interfaces*, **8**, 25229 (2016).
22. L. L. Baranowski, C. M. Heveran, V. L. Ferguson, and C. R. Stoldt, "Multi-scale mechanical behavior of the Li3PS4 solid-phase electrolyte." *ACS applied materials & interfaces*, **8**, 29573 (2016).

23. A. Sakuda, A. Hayashi, Y. Takigawa, K. Higashi, and M. Tatsumisago, "Evaluation of elastic modulus of Li2SP2S5 glassy solid electrolyte by ultrasonic sound velocity measurement and compression test." *J. Ceram. Soc. Jpn.*, **121**, 946 (2013).
24. Z. Lin, Z. Liu, W. Fu, N. J. Dudney, and C. Liang, "Lithium polysulfidophosphates: a family of lithium-conducting sulfur-rich compounds for lithiumsulfur batteries." *Angew. Chem. Int. Ed.*, **52**, 7460 (2013).
25. F. Shen, M. B. Dixit, W. Zaman, N. Hortance, B. Rogers, and K. B. Hatzell, "Composite electrode ink formulation for all solid-state batteries." *J. Electrochem. Soc.*, **166**, A3182 (2019).
26. K. B. Hatzell and Y. Zheng, "Prospects on large-scale manufacturing of solid state batteries." *MRS Energy & Sustainability*, **8**, 33 (2021).
27. R. Xu, J. Yue, S. Liu, J. Tu, F. Han, P. Liu, and C. Wang, "Cathode-supported all-solidstate lithiumsulfur batteries with high cell-level energy density." *ACS Energy Lett.*, **4**, 1073 (2019).
28. X. Judez, H. Zhang, C. Li, G. G. Eshetu, J. A. Gonzalez-Marcos, M. Armand, and L. M. Rodriguez-Martinez, "Solid electrolytes for safe and high energy density lithiumsulfur batteries: promises and challenges." *J. Electrochem. Soc.*, **165**, A6008 (2017).
29. L. Sang, K. L. Bassett, F. C. Castro, M. J. Young, L. Chen, R. T. Haasch, J. W. Elam, V. P. Dravid, R. G. Nuzzo, and A. A. Gewirth, "Understanding the effect of interlayers at the thiophosphate solid electrolyte/lithium interface for all-solid-state Li batteries." *Chemistry of Materials*, **30**, 8747 (2018).
30. M. B. Dixit, A. Verma, W. Zaman, X. Zhong, P. Kenesei, J. S. Park, J. Almer, P. P. Mukherjee, and K. B. Hatzell, "Synchrotron Imaging of Pore Formation in Li Metal Solid-State Batteries Aided by Machine Learning." *ACS Appl. Energy Mater.*, **3**, 9534 (2020).
31. W. Zhou, Y. Yu, H. Chen, F. J. DiSalvo, and H. D. Abrun a, "Yolkshell structure of polyaniline-coated sulfur for lithiumsulfur batteries." *J. Am. Chem. Soc.*, **135**, 16736 (2013).
32. Y. Ren, N. Hortance, J. McBride, and K. B. Hatzell, "SodiumSulfur Batteries Enabled by a Protected Inorganic/Organic Hybrid Solid Electrolyte." *ACS Energy Lett.*, **6**, 345 (2020).
33. D. Hlushkou, A. E. Reising, N. Kaiser, S. Spannenberger, S. Schlabach, Y. Kato, B. Roling, and U. Tallarek, "The influence of void space on ion transport in a composite cathode for all-solid-state batteries." *Journal of Power Sources*, **396**, 363 (2018).
34. A. Bielefeld, D. A. Weber, and J. Janek, "Modeling Effective Ionic Conductivity and Binder Influence in Composite Cathodes for All-Solid-State Batteries." *ACS Applied Materials & Interfaces*, **12**, 12821 (2020).
35. M. B. Dixit et al., "Nanoscale mapping of extrinsic interfaces in hybrid solid electrolytes." *Joule*, **4**, 207 (2020).
36. W. Zaman, N. Hortance, M. B. Dixit, V. De Andrade, and K. B. Hatzell, "Visualizing percolation and ion transport in hybrid solid electrolytes for Limetal batteries." *Journal of Materials Chemistry A*, **7**, 23914 (2019).
37. R. Koerver, I. Aygun, T. Leichtweiß, C. Dietrich, W. Zhang, J. O. Binder, P. Hartmann, W. G. Zeier, and J. Janek, "Capacity fade in solid-state batteries: interphase formation and chemomechanical processes in nickel-rich layered oxide cathodes and lithium thiophosphate solid electrolytes." *Chemistry of Materials*, **29**, 5574 (2017).
38. D. Y. Oh, Y. J. Nam, K. H. Park, S. H. Jung, S.-J. Cho, Y. K. Kim, Y.-G. Lee, S.-Y. Lee, and Y. S. Jung, "Excellent Compatibility of Solvate Ionic Liquids with Sulfide Solid Electrolytes: Toward Favorable Ionic Contacts in Bulk-Type All-Solid-State Lithium-Ion Batteries." *Adv. Energy Mater.*, **5**, 1500865 (2015).
39. Z. Jiang et al., "Machine-learning-revealed statistics of the particle-carbon/binder detachment in lithium-ion battery cathodes." *Nat. Commun.*, **11**, 1 (2020).
40. M. Liu, D. Zhou, Y.-B. He, Y. Fu, X. Qin, C. Miao, H. Du, B. Li, Q.-H. Yang, and Z. Lin, "Novel gel polymer electrolyte for high-performance lithiumsulfur batteries." *Nano Energy*, **22**, 278 (2016).
41. D. P. Nair, M. Podgorski, S. Chatani, T. Gong, W. Xi, C. R. Fenoli, and C. N. Bowman, "The thiol-Michael addition click reaction: a powerful and widely used tool in materials chemistry." *Chemistry of Materials*, **26**, 724 (2013).
42. B. D. Mather, K. Viswanathan, K. M. Miller, and T. E. Long, "Michael addition reactions in macromolecular design for emerging technologies." *Progress in Polymer Science*, **31**, 487 (2006).
43. K. Dokko et al., "Solvate ionic liquid electrolyte for LiS batteries." *J. Electrochem. Soc.*, **160**, A1304 (2013).
44. D. Y. Oh, Y. J. Nam, K. H. Park, S. H. Jung, S.-J. Cho, Y. K. Kim, Y.-G. Lee, S.-Y. Lee, and Y. S. Jung, "Excellent Compatibility of Solvate Ionic Liquids with Sulfide-Solid Electrolytes: Toward Favorable Ionic Contacts in Bulk-Type All-Solid-State Lithium-Ion Batteries." *Adv. Energy Mater.*, **5**, 1500865 (2015).
45. Y. Ren, L. Zeng, H. Jiang, W. Ruan, Q. Chen, and T. Zhao, "Rational design of spontaneous reactions for protecting porous lithium electrodes in lithiumsulfur batteries." *Nat. Commun.*, **10**, 1 (2019).
46. R. Xu, J. Yue, S. Liu, J. Tu, F. Han, P. Liu, and C. Wang, "Cathode-supported all-solidstate lithiumsulfur batteries with high cell-level energy density." *ACS Energy Lett.*, **4**, 1073 (2019).
47. D. Y. Oh, Y. J. Nam, K. H. Park, S. H. Jung, K. T. Kim, A. R. Ha, and Y. S. Jung, "Slurry-Fabricable Li^+-Conductive Polymeric Binders for Practical All- Solid-State Lithium-Ion Batteries Enabled by Solvate Ionic Liquids." *Adv. Energy Mater.*, **9**, 1802927 (2019).
48. T. Swamy, X. Chen, and Y.-M. Chiang, "Electrochemical redox behavior of li ion conducting sulfide solid electrolytes." *Chemistry of Materials*, **31**, 707 (2019).
49. F. Han, A. S. Westover, J. Yue, X. Fan, F. Wang, M. Chi, D. N. Leonard, N. J. Dudney, H. Wang, and C. Wang, "High electronic conductivity as the origin of lithium dendrite formation within solid electrolytes." *Nat. Energy*, **4**, 187 (2019).
50. K. Takada, M. Osada, N. Ohta, T. Inada, A. Kajiyama, H. Sasaki, S. Kondo, M. Watanabe, and T. Sasaki, "Lithium ion conductive oxysulfide, Li3PO4Li3PS4." *Solid State Ionics*, **176**, 2355 (2005).
51. S. Zhang, K. Zhao, T. Zhu, and J. Li, "Electrochemomechanical degradation of highcapacity battery electrode materials." *Prog. Mater. Sci.*, **89**, 479 (2017).